THE JOURNAL OF BIOLOGICAL CHEMISTRY VOL. 287, NO. 16, pp. 13128–13136, April 13, 2012

Phosphatidylinositol 5-Phosphatase Oculocerebrorenal Syndrome of Lowe Protein (OCRL) Controls Actin Dynamics during Early Steps of *Listeria monocytogenes* Infection*[S]

Received for publication, October 20, 2011, and in revised form, February 9, 2012 Published, JBC Papers in Press, February 18, 2012, DOI 10.1074/jbc.M111.315788

Andreas Kühbacher[‡§¶1], **Daphné Dambournet**[‖**‡‡2], **Arnaud Echard**[‖**], **Pascale Cossart**[‡§¶], **and Javier Pizarro-Cerdá**[‡§¶3]

From the [‡]*Unité des Interactions Bactéries Cellules, Institut Pasteur, F-75015 Paris,* [§]*INSERM U604, F-75015 Paris, the* [¶]*Institut National de la Recherche Agronomique (INRA), USC2020, F-75015 Paris,* [‡‡]*Université Pierre et Marie Curie, Cellule Pasteur UPMC, F-75015 Paris, the* [‖]*Unité Traffic Membranaire et Division Cellulaire, Institut Pasteur, F-75015 Paris, and the* **CNRS URA2582, F-75015 Paris, France*

Background: OCRL is a 5-phosphatase that dephosphorylates $PI(4,5)P_2$ and $PI(3,4,5)P_3$.
Results: OCRL knockdown by siRNA increases cell invasion by *Listeria monocytogenes*.
Conclusion: $PI(4,5)P_2$ and $PI(3,4,5)P_3$ pools controlled by OCRL regulate actin dynamics during *L. monocytogenes* invasion.
Significance: OCRL is the first eukaryotic lipid phosphatase implicated in a bacterial invasion process.

Listeria monocytogenes **is a bacterial pathogen that induces its own entry into a broad range of mammalian cells through interaction of the bacterial surface protein InlB with the cellular receptor Met, promoting an actin polymerization/depolymerization process that leads to pathogen engulfment. Phosphatidylinositol bisphosphate ($PI[4,5]P_2$) and trisphosphate ($PI[3,4,5]P_3$) are two major phosphoinositide species that function as molecular scaffolds, recruiting cellular effectors that regulate actin dynamics during *L. monocytogenes* infection. Because the phosphatidylinositol 5′-phosphatase OCRL dephosphorylates $PI(4,5)P_2$ and to a lesser extent $PI(3,4,5)P_3$, we investigated whether this phosphatase modulates cell invasion by *L. monocytogenes*. Inactivation of OCRL by small interfering RNA (siRNA) leads to an increase in the internalization levels of *L. monocytogenes* in HeLa cells. Interestingly, OCRL depletion does not increase but rather decreases the surface expression of the receptor Met, suggesting that OCRL controls bacterial internalization by modulating signaling cascades downstream of Met. Immuno-fluorescence microscopy reveals that endogenous and overexpressed OCRL are present at *L. monocytogenes* invasion foci; live-cell imaging additionally shows that actin depolymerization coincides with EGFP-OCRL-a accumulation around invading bacteria. Together, these observations suggest that OCRL promotes actin depolymerization during *L. monocytogenes* infection; in agreement with this hypothesis, OCRL depletion leads to an increase in actin, $PI(4,5)P_2$, and $PI(3,4,5)P_3$ levels at bacterial internalization foci. Furthermore, in cells knocked down for OCRL, transfection of enzymatically active EGFP-OCRL-a (but not of a phosphatase-dead enzyme) decreases the levels of intracellular *L. monocytogenes* and of actin associated with invading bacteria. These results demonstrate that through its phosphatase activity, OCRL restricts *L. monocytogenes* invasion by modulating actin dynamics at bacterial internalization sites.**

The Gram-positive bacterial pathogen *Listeria monocytogenes* is responsible for a food-borne infection characterized by diverse clinical outcomes including gastroenteritis, meningitis, and abortion (1); the capacity of *L. monocytogenes* to induce illness is highly related to its ability to invade the intracellular space of host cells (2). Bacterially induced cellular invasion is accomplished through interaction of the cellular receptors E-cadherin and Met with the *L. monocytogenes* surface proteins InlA and InlB, respectively (3, 4), which activate signaling cascades that ultimately lead to actin rearrangements responsible for plasma membrane remodeling and bacterial internalization (5). Manipulation of the phosphoinositide metabolism is a major mechanism by which *L. monocytogenes* subverts cellular functions to promote entry (6). InlB is the first reported non-mammalian agonist of the phosphatidylinositol (PI) 3-kinase p85-p110 (7, 8), and production of $PI(3,4,5)P_3$[4] promotes the activation of Rac1 (9) and of WASP family members upstream of actin polymerization by the Arp2/3 complex (10). The InlB/Met interaction is also responsible for the production of phosphatidylinositol 4-phosphate by type II PI 4-kinases, which modulate a PI 3-kinase-independent pathway to favor cellular invasion by *L. monocytogenes* (11).

Although the role of lipid kinases during *L. monocytogenes* infection has been documented (7, 11), the role of lipid

* This work was supported by the Pasteur Institute, the European Research Council Grant 233348, INSERM, INRA, CNRS, the Louis-Jeantet Foundation, La Fondation Le Roch-Les Mousquetaires, Agence Nationale de la Recherche Grant ANR-09-MIEN-020 (to P. C.) and Grant ANR-07-JCJC-0089 (to A. E.), and the Schlumberger Foundation for Education and Research (to A. E.).

[S] This article contains supplemental Figs. S1–S3.

[1] Recipient of a scholarship from the Pasteur-Paris University International Doctoral Program/Institut Carnot Maladies Infectieuses.

[2] Supported by the Ministère de la Recherche et de l'Enseignement Supérieur and by the Association pour la Recherche sur le Cancer.

[3] To whom correspondence should be addressed: Institut Pasteur, Unité des Interactions Bactéries-Cellules, INSERM U604, INRA USC2020, 28 rue du Docteur Roux, 75724 Paris Cedex 15, France. Tel.: 33-4061-3779; Fax: 33-4568-8706; E-mail: pizarroj@pasteur.fr.

[4] The abbreviations used are: $PI(3,4,5)P_3$, phosphatidylinositol trisphosphate; $PI(4,5)P_2$, phosphatidylinositol bisphosphate; OCRL, oculocerebrorenal syndrome of Lowe protein; WASP, Wiskott–Aldrich syndrome protein; EGFP, enhanced green fluorescent protein.

phosphatases has not yet been addressed. OCRL is a 5′-phosphatase that dephosphorylates preferentially $PI(4,5)P_2$ but also $PI(3,4,5)P_3$ to a lesser extent (12), and its gene is mutated in patients suffering from a rare X-linked genetic disease known as oculocerebrorenal syndrome of Lowe, characterized by defects of the nervous system, the eye, and the kidney (13). Several recent studies have highlighted specific functions of this 5′-phosphatase in diverse cellular processes. For example, OCRL has been shown to interact with clathrin and to participate in early steps of the endocytic pathway (14–18); OCRL also controls $PI(4,5)P_2$ levels and promotes local actin depolymerization required for successful cytokinesis (19, 20). We investigated whether OCRL could modulate the entry of *L. monocytogenes* in HeLa cells and observed that OCRL knockdown leads to a significant increase in bacterial infection. We also showed that OCRL is recruited to *L. monocytogenes* internalization foci when actin depolymerization takes place at these structures. Analysis of the association of actin and phosphoinositides to invading *L. monocytogenes* in wild type and OCRL-depleted cells leads us to propose that by reducing the levels of $PI(4,5)P_2$ and $PI(3,4,5)P_3$ at the plasma membrane, OCRL restricts infection through modulation of actin dynamics at bacterial internalization sites.

EXPERIMENTAL PROCEDURES

Cell Culture and Bacteria—HeLa American Type Culture Collection (ATCC) CCL-2 cells were cultured at 37 °C in a humidified 10% CO_2 atmosphere in DMEM supplemented with 10% fetal calf serum (FCS). *L. monocytogenes* strains EGD, EGD ΔInlA, EGD ΔInlB, P14, and P14.PrfA* were grown overnight at 37 °C in 5 ml of brain heart infusion medium (Difco Laboratories). Bacteria were washed three times with PBS before use to remove secreted listeriolysin O. Infections were carried out in DMEM supplemented with 1% FCS.

Antibodies, Probes, and Plasmids—For immuno-fluorescence staining or Western blot experiments, the following primary antibodies were used: R11 primary rabbit serum against heat-killed *L. monocytogenes* EGD, rabbit anti-OCRL (19), rabbit anti-Met (C-12, Santa Cruz Biotechnology), mouse anti-Met (DO-24, Upstate Biotech Millipore), mouse anti-glyceraldehyde-3-phosphate dehydrogenase (GAPDH: 6C5, Abcam), and mouse anti-actin (AC15, Sigma-Aldrich). Primary rabbit serum against heat-killed *L. monocytogenes* P14 (R217) was produced as follows. Bacteria were grown to $A_{600} = 1$, centrifuged, and washed with phosphate buffer (pH 7.4). Concentration was adjusted to 5×10^{10} bacteria/ml, and the suspension was heated at 60 °C for 1 h. 5×10^9 killed bacteria were emulsified with incomplete Freund's adjuvant and injected subcutaneously into rabbits. 6 and 12 weeks after the first immunization, animals were boosted following the same immunization protocol. Rabbits were finally bled 10 days after the third boost. Secondary antibodies for immuno-fluorescence staining were goat anti-rabbit or goat anti-mouse antibodies conjugated with Alexa Fluor 488, Alexa Fluor 350, or Alexa Fluor 546 (Molecular Probes). Secondary antibodies for Western blot were peroxidase-coupled anti-mouse and anti-rabbit sera (AbCys). F-actin was labeled with phalloidin-Alexa Fluor 647, DNA was labeled with Hoechst, and plasma membrane was labeled with wheat germ agglutinin-Alexa Fluor 555 (Molecular Probes). For protein expression, the following plasmids were used: EGFP-OCRL-a (Dr. F. Nagano, Curie Institute), EGFP-OCRL-a and EGFP-OCRL-a H507R (both siRNA-resistant) (19), EGFP (Clontech), LifeAct-cherry, PH-PLC-δ-3-cherry, and PH-AKT-citrine (9). Transfection was performed using the liposome-based FuGENE HD transfection procedure (Roche Applied Science) according to the manufacturer's protocol. Plasmids were used at a final concentration of 0.5 μg/ml, and the transfection reagent was used at a final concentration of 0.3%. Transfections were carried out 18–24 h before the experiment in 24-well plates (Techno Plastic Products AG).

RNA Interference—HeLa cells were transfected with siRNA targeting OCRL (5′-GAAAGGAUCAGUGUCGAUA-3′ synthesized by Eurogentec after a SMARTpool sequence from Dharmacon) or noncoding siRNA control (Silencer Negative Control #1, Ambion) at a concentration of 50 nM for 72 h. Lipofectamine RNAiMAX (Invitrogen) was used at a final concentration of 0.1%, and knockdown efficiency was tested by Western blot using the ECL Plus kit (Pierce).

Gentamicin Invasion Assay—L. monocytogenes invasion was measured performing gentamicin invasion assays as described previously (21). Briefly, HeLa cells plated the day before or transfected with siRNA 72 h before in 24-well plates were infected with *L. monocytogenes* at multiplicity of infection 5 (P14.PrfA*) or 50 (P14, EGD, EGD ΔInlA, EGD ΔInlB) for 1 h. Subsequently, extracellular bacteria were killed by treatment with 25 μg/ml of the non-cell-permeable antibiotic gentamicin for an additional hour. After lysis of the cells with distilled water and plating of the lysates on brain heart infusion agar plates, colonies were counted to calculate the number of intracellular bacteria.

Immunofluorescence Staining and Microscopy—For fluorescence microscopy, cells were plated in 24-well plates on coverslips at a density of 20,000–50,000 cells per well. After infection with *L. monocytogenes* at multiplicity of infection 25–50 for P14.PrfA* or multiplicity of infection 100 for P14, centrifugation for 5 min at 1000 rpm, and incubation at 37 °C for the individually indicated time, cells were fixed with 4% paraformaldehyde in phosphate-buffered saline (PBS) for 15 min. The antibodies against OCRL (rabbit) and Met (C-12, rabbit) were used at a dilution of 1:100 in PBS supplemented with 1% bovine serum albumin (BSA) and 0.05% saponin. Rabbit-derived antibodies for staining of *L. monocytogenes* were used at a dilution of 1:300 in PBS supplemented with 1% BSA without saponin for staining of extracellular bacteria or with 0.05% saponin for staining of total bacteria. Secondary fluorophore-coupled antibodies were used at 1:200 in PBS supplemented with 1% BSA with or without 0.05% saponin. F-actin was stained by fluorescent phalloidin and plasma membrane was stained with fluorescent wheat germ agglutinin, both of which were diluted 1:100. All antibody incubation times were between 30 and 60 min. Coverslips processed for immuno-fluorescence were mounted on microscopy glass slides using 5 μl of Fluoromount G (Interchim), and images were acquired using an 100× objective mounted on an inverted wide-field fluorescence microscope (AxioVert 200M, Carl Zeiss Microscopy) equipped with a digital camera (CoolSNAP HQ^2, Photometrics) and the software MetaMorph (Molecular Devices). Background noise was

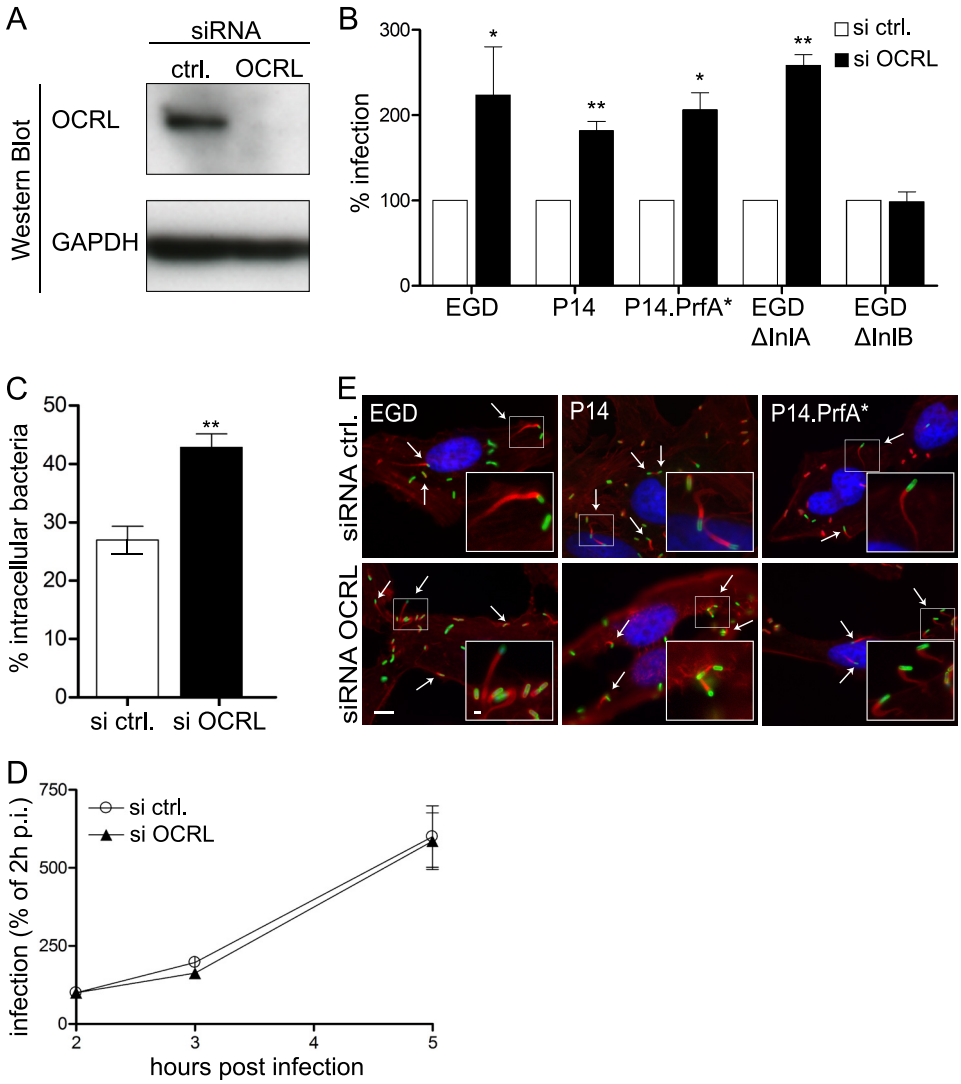

FIGURE 1. **OCRL depletion promotes *L. monocytogenes* invasion of HeLa cells.** *A*, OCRL expression was knocked down in HeLa cells for 72 h using specific siRNA oligonucleotides, and protein levels were verified by Western blot employing GAPDH as a loading control. *siRNA ctrl.*, siRNA control. *B*, gentamicin invasion assays were performed in HeLa cells transfected with control or anti-OCRL siRNA using five different *L. monocytogenes* strains: EGD, P14, P14.PrfA*, EGD ΔInlA, and EGD ΔInlB. Values represent the averages ± S.E. of tetraplicate samples from 3–4 independent experiments (Student's *t* test: *, $p < 0.05$ and **, $p < 0.01$). *C*, HeLa cells transfected with control or anti-OCRL siRNA were infected for 1 h with *L. monocytogenes* P14.PrfA* strain, and cells were processed for immuno-fluorescence microscopy with specific labeling of total *versus* extracellular bacteria. Values represent the averages ± S.E. of 3 independent experiments ($n = 200$ bacteria analyzed per experiment; Student's *t* test: **, $p < 0.01$). *D*, gentamicin invasion assays for *L. monocytogenes* EGD were done in OCRL-depleted and control cells at 2, 3, and 5 h after infection to monitor intracellular growth. Values represent the averages ± S.E. of tetraplicate samples from one representative experiment out of two independent experiments. *p.i.*, post-infection. *E*, cells knocked down for OCRL or transfected with control siRNA were infected with the indicated *L. monocytogenes* strains. Cells were processed for immuno-fluorescence. DNA was labeled with Hoechst (*blue*), *L. monocytogenes* were labeled with antibodies against the bacterial cell wall (*green*), and actin comet tails polymerized by intracellular bacteria (*arrows*) were labeled with fluorescent phalloidin (*red*). *Bar*: 10 μm (*inset bar*: 1 μm).

removed by background subtraction using ImageJ and applying a despeckle filter using Photoshop (Adobe). For live-cell microscopy cells, were plated in glass bottom 35-mm dishes (Mattek) and transfected 24 h before use. Prior to movie acquisition, bacteria were added, and the dishes were centrifuged at room temperature for 5 min at 1000 rpm. Images were taken every 20–45 s after transfer of the dishes to a prewarmed (37 °C) AxioVert 200M, to a spinning disc system (PerkinElmer Life Sciences) equipped with a digital ORCA II ER camera (Hamamatsu). For some live-cell imaging experiments, cells were grown on 384 well plates (Greiner) and imaged on an ImageXpress microscope (Molecular Devices).

Image Quantification—Invasion was quantified by counting extracellular bacteria, visualized by bacterial staining prior to cell permeabilization, and counting total bacteria associated to cells, visualized by bacterial staining after permeabilization of the cells. Subsequently, invasion was calculated as the ratio of intracellular to total bacteria. The numbers of bacteria associated to transfected markers were counted by ocular inspection, and the ratio with intracellular or pEGFP-OCRL-a-positive bacteria was calculated. In each case, experiments have been repeated at least three times, and 25–800 bacteria were counted for each data point and replicate. Cellular GFP intensities were measured using ImageJ.

Flow Cytometry—For flow cytometry-based analysis of surface Met expression, cells knocked down for OCRL or control siRNA treated for 72 h were detached with trypsin, fixed with

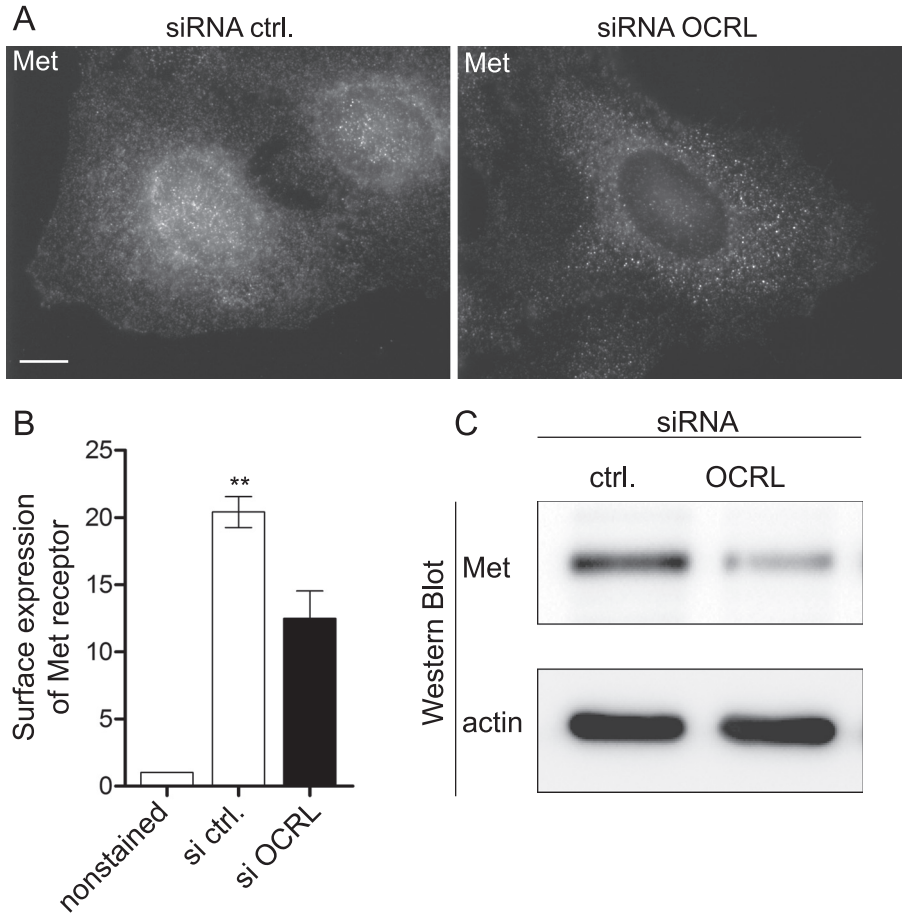

FIGURE 2. **OCRL depletion decreases expression of Met.** *A*, after 72 h of transfection with control or anti-OCRL siRNA, HeLa cells were fixed and processed for immuno-fluorescence microscopy in saponin permeabilized cells using the anti-Met C-12 antibody. *Bar*: 10 μm. *siRNA ctrl.*, siRNA control. *B*, surface expression of Met in control and OCRL-depleted cells was quantified by flow cytometry without cellular permeabilization using the DO-24 antibody against the extracellular moiety of Met. The results represents the -fold change of geometric mean as compared with unstained cells $\pm$ S.E. of 3 independent experiments (Student's *t* test: **, $p < 0.01$). *C*, expression of Met in control and OCRL-depleted cells was verified by Western blot using the anti-Met C-12 antibody.

4% paraformaldehyde in PBS for 30 min on ice, and stained with an anti-Met primary antibody (DO-24) 1:100 in PBS suplemented with 1% BSA and a secondary Alexa Fluor 488-coupled anti-mouse antibody, both for 1 h. The Alexa Fluor 488 fluorescent signal was measured using a FACSCalibur flow cytometer (BD Biosciences). Dead cells were excluded by gating for the living cell population. 10,000 cells were counted for each sample.

RESULTS

OCRL Depletion Promotes L. monocytogenes Invasion of HeLa Cells—To evaluate a potential role of OCRL in cell invasion by *L. monocytogenes*, we inactivated this phosphatase by siRNA transfection in HeLa cells (Fig. 1*A*) and performed gentamicin invasion assays using five bacterial strains: wild type EGD strain serotype 1/2b, EGD ΔInlA, EGD ΔInlB, wild type P14 strain serotype 4b, and a hyperinvasive P14.PrfA* strain. As shown in Fig. 1*B*, inactivation of OCRL doubles the number of intracellular EGD strain after 1 h of bacterial infection followed by 1 h of gentamicin treatment to kill extracellular microorganisms. Similar results were observed using the P14 and P14.PrfA* strains (Fig. 1*B* and supplemental Fig. S1), indicating that our results are not restricted to one specific *L. monocytogenes* strain. OCRL knockdown promotes the increase of the EGD ΔInlA strain intracellular counts but has no effect on the background entry levels of the EGD ΔInlB strain (Fig. 1*B* and supplemental Fig. S1), indicating that OCRL modulates the Met/InlB-dependent invasion pathway. We further assessed by microscopy the effect of OCRL inactivation on *L. monocytogenes* entry and confirmed that more intracellular bacteria are detected in OCRL-depleted cells in comparison with cells treated with control siRNA after 1 h of infection (Fig. 1*C*). To investigate whether OCRL knockdown affects the *L. monocytogenes* entry step into target cells or whether OCRL modulates bacterial intracellular proliferation, we quantified in gentamicin invasion assays the number of intracellular bacteria at 2, 3, and 5 h after infection. As shown in Fig. 1*D*, we did not observe differences in the bacterial intracellular replication rates between control and OCRL-depleted cells, suggesting that OCRL knockdown specifically enhances the entry of *L. monocytogenes* into host cells. To verify that bacterial post-entry steps are not affected in cells inactivated for OCRL, we assessed the formation of actin comet tails by intracellular *L. monocytogenes* in control and OCRL-depleted cells 5 h after infection. We observed that bacteria are still able to polymerize cytoplasmic actin in cells inactivated for OCRL (Fig. 1*E*), demonstrating

that bacteria are able to reach their final intracellular target compartment in cells lacking OCRL and that the infection process is productive in these cells. Altogether, these results demonstrate that inactivation of OCRL promotes the entry of *L. monocytogenes* in HeLa cells.

OCRL Depletion Does Not Increase Surface Expression of Met—One potential mechanism by which OCRL depletion could modulate the efficiency of *L. monocytogenes* invasion in HeLa cells is by modifying the surface expression of the InlB receptor Met. Indeed, OCRL function has been linked to receptor endocytosis (16) as well as receptor sorting and recycling in the endocytic pathway (18). We therefore examined the distribution and expression of Met in control and OCRL-depleted cells to evaluate the hypothesis that OCRL inactivation could potentially lead to an increase in the surface expression of Met and therefore facilitate bacterial entry. Using the C-12 antibody, which recognizes the intracellular moiety of the Met β-chain, by immuno-fluorescence microscopy, we observed in control cells a strong and fine Met signal that is distributed along the whole cell body including the cell periphery and the perinuclear area. In contrast, in OCRL-depleted cells, we observed a weaker Met signal that is confined to bigger punctate structures (Fig. 2*A*). By flow cytometry of nonpermeabilized cells using the DO-24 antibody, which recognizes the extracellular moiety of Met, we could show that OCRL depletion leads to a significant ($p < 0.01$) reduction of Met surface levels in HeLa cells (Fig. 2*B*). Western blot of whole cell lysates confirms an important global reduction of Met levels in OCRL siRNA-treated HeLa cells (Fig. 2*C*). Therefore, OCRL inactivation does not increase but rather decreases the levels of Met receptors available for interaction with the bacterial invasion protein InlB, suggesting that the augmented *L. monocytogenes* invasion upon OCRL siRNA knockdown relies on an active mechanism directly related to cell signaling downstream of Met.

OCRL Is Recruited to L. monocytogenes Invasion Foci—To understand how OCRL modulates the entry of *L. monocytogenes* in target cells, we investigated the cellular distribution of the lipid phosphatase in infected HeLa cells by immuno-fluorescence microscopy. Using an antibody against endogenous OCRL, we were able to detect an enrichment of OCRL-positive structures at sites of bacterial internalization at 10 min after infection (Fig. 3*A* and supplemental Fig. S2*A*). Transfection of HeLa cells with an EGFP-tagged version of OCRL-a leads to a more pronounced association of the lipid phosphatase to the *L. monocytogenes* internalization foci (Fig. 3*B* and supplemental Fig. S3*A*). Plasma membrane labeling with the fluorescently tagged lectin wheat germ agglutinin shows that OCRL accumulation around invading bacteria does not always colocalize with the plasma membrane marker (supplemental Fig. S2), suggesting that OCRL labeling is specific and does not necessarily appear whenever plasma membrane accumulation is detected. Performing an immuno-labeling experiment, which differentiates extracellular and partially internalized *versus* total bacteria, we showed that GFP-tagged OCRL-a is mainly associated to fully internalized *L. monocytogenes* (Fig. 3*B*). Quantification of the relative ratio of extracellular *versus* intracellular bacteria, which are labeled by

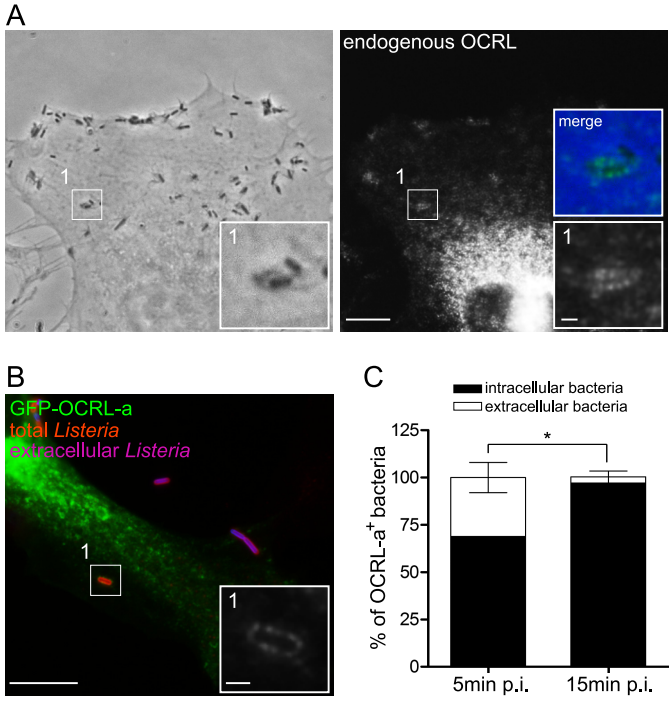

FIGURE 3. **OCRL is recruited to *L. monocytogenes* internalization sites.** *A*, HeLa cells were infected for 10 min with *L. monocytogenes* P14.PrfA* and processed for immuno-fluorescence microscopy by labeling endogenous OCRL. *Bar*: 10 μm (*inset bar*: 1 μm). *B*, HeLa cells were transfected for 24 h with EGFP-OCRL-a (*green*) and were subsequently infected for 10 min with *L. monocytogenes* P14.PrfA*; cells were then processed for fluorescence microscopy with differential labeling of extracellular (*blue*) and total bacteria (*red*). The *inset* highlights a specific area of the EGFP-OCRL-a channel. *Bar*: 10 μm (*inset bar*: 1 μm). *C*, quantification of the proportion of intracellular *versus* extracellular bacteria that were labeled by the EGFP-OCRL-a marker in cells processed for *B*. Values represent the averages ± S.E. of 3 independent experiments (Student's *t* test: *, $p < 0.05$). *p.i.*, post-infection.

EGFP-OCRL-a, indicates that almost 70% of the EGFP-OCRL-a-positive bacteria are intracellular at 5 min after bacterial inoculation; this value increases to 96% at 15 min after infection (Fig. 3*C*). These results demonstrate that OCRL is recruited to *L. monocytogenes* invasion foci during the very early stages of bacterial internalization in HeLa cells.

Actin Polymerization Precedes OCRL Recruitment to L. monocytogenes Invasion Foci—Because the lipid phosphatase activity of OCRL has been described as a modifier of the plasma membrane levels of $PI(4,5)P_2$ (12), which is itself an important regulator of actin polymerization, we investigated the distribution of actin and pEGFP-OCRL-a during *L. monocytogenes* internalization. At 10 min after infection, we detected bacteria that were positive for endogenous OCRL or EGFP-OCRL-a but not for actin (Fig. 4*A*). Quantification of EGFP-OCRL-a- and actin-positive bacteria by immuno-fluorescence microscopy revealed that double-positive bacteria were only abundant during the first minutes of infection; at later time points, larger bacterial numbers were found positive for EGFP-OCRL-a but negative for actin (Fig. 4*B*), showing that presence of actin is inversely correlated to EGFP-OCRL-a presence around invading bacteria. Live-cell imaging of HeLa cells transfected with EGFP-OCRL-a and LifeAct-Cherry (a fluorescent probe that labels F-actin) revealed that

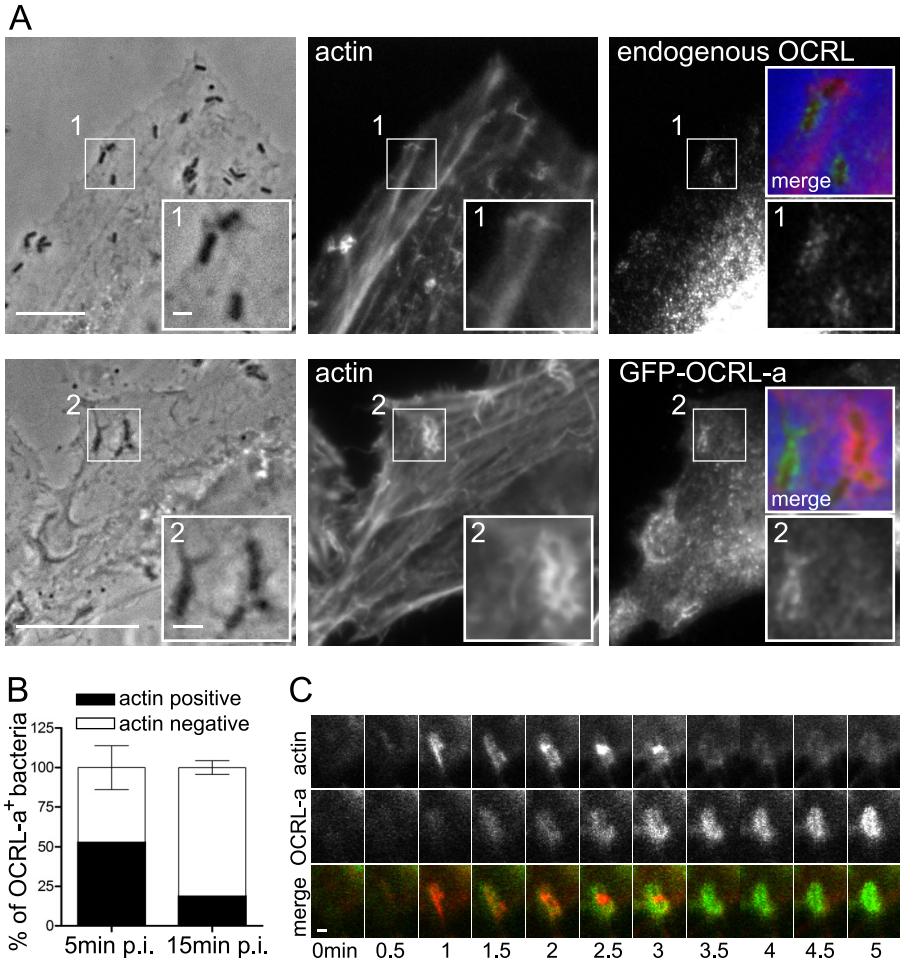

FIGURE 4. **Actin polymerization precedes OCRL recruitment to *L. monocytogenes* vacuoles.** *A*, microscopy analysis of the distribution of endogenous OCRL, EGFP-OCRL-a, and actin in cells infected by *L. monocytogenes* P14.PrfA*. *Bar*: 10 μm (*inset bar*: 1 μm). *B*, quantification of the recruitment of OCRL and actin by *L. monocytogenes* P14.PrfA*. Values represent the averages ± S.E. of 3 independent experiments. *p.i.*, post-infection. *C*, live-cell imaging illustrating the sequential recruitment of actin visualized by LifeAct-cherry and OCRL by *L. monocytogenes* P14.PrfA*. *Bar*: 1 μm.

actin polymerization precedes EGFP-OCRL-a recruitment to bacterial internalization sites (Fig. 4*C*). Altogether, these results suggest that OCRL recruitment to *L. monocytogenes* invasion foci could be implicated in the depolymerization of actin upon bacterial internalization.

OCRL Depletion Restricts Actin Depolymerization at L. monocytogenes Invasion Foci—To verify that OCRL function could regulate actin dynamics during the *L. monocytogenes* invasion process, we inactivated OCRL by targeted siRNA transfection and analyzed the association of actin to bacteria-containing compartments by immuno-fluorescence wide-field microscopy in fixed HeLa cells. As shown in Fig. 5*A*, depletion of OCRL leads to an increase in the number of invading *L. monocytogenes* associated to actin at 15 min after infection. Moreover, by time-lapse microscopy in living cells, we observed that the average duration of actin association to invading bacteria increases from 5 min in control cells to 14 min in cells inactivated for OCRL (Fig. 5*B*). Because, as mentioned above, OCRL major substrates are $PI(4,5)P_2$ and $PI(3,4,5)P_3$, we investigated whether OCRL depletion could modify the association of these phosphoinositides to invading *L. monocytogenes*. $PI(4,5)P_2$ and $PI(3,4,5)P_3$, visualized using the probes PH-PLCδ-3-Cherry and PH-AKT-citrine, respectively, were detected at bacterial entry sites (Fig. 5 and supplemental Fig. S3). As shown in Fig. 5, *E* and *F*, we observed that larger numbers of $PI(4,5)P_2$- and $PI(3,4,5)P_3$-positive bacteria are detected in OCRL-depleted cells in comparison with control cells. Our results therefore suggest that by decreasing the levels of $PI(4,5)P_2$ and $PI(3,4,5)P_3$, OCRL coordinates the depolymerization of actin during *L. monocytogenes* invasion of target cells.

OCRL Phosphatase Function Is Responsible for Restricting L. monocytogenes Invasion and for Promoting Actin Depolymerization at Bacterial Entry Foci—To definitively establish a direct link between the OCRL phosphatase function and actin depolymerization at *L. monocytogenes* internalization sites, we inactivated OCRL in HeLa cells and additionally transfected these cells either with wild type EGFP-OCRL-a or with the EGFP-OCRL-a H507R mutant form devoid of phosphatase activity (both OCRL versions are siRNA-resistant) to assess by immuno-fluorescence microscopy the numbers of intracellular bacteria and the levels of actin association to bacteria-containing compartments. As shown in Fig. 6*A*, transfection and overexpression of wild type EGFP-OCRL-a in OCRL-depleted cells lead to a decrease in the numbers of intracellular bacteria, whereas transfection of the EGFP-OCRL-a H507R phosphatase-dead mutant does not rescue the knockdown effect as

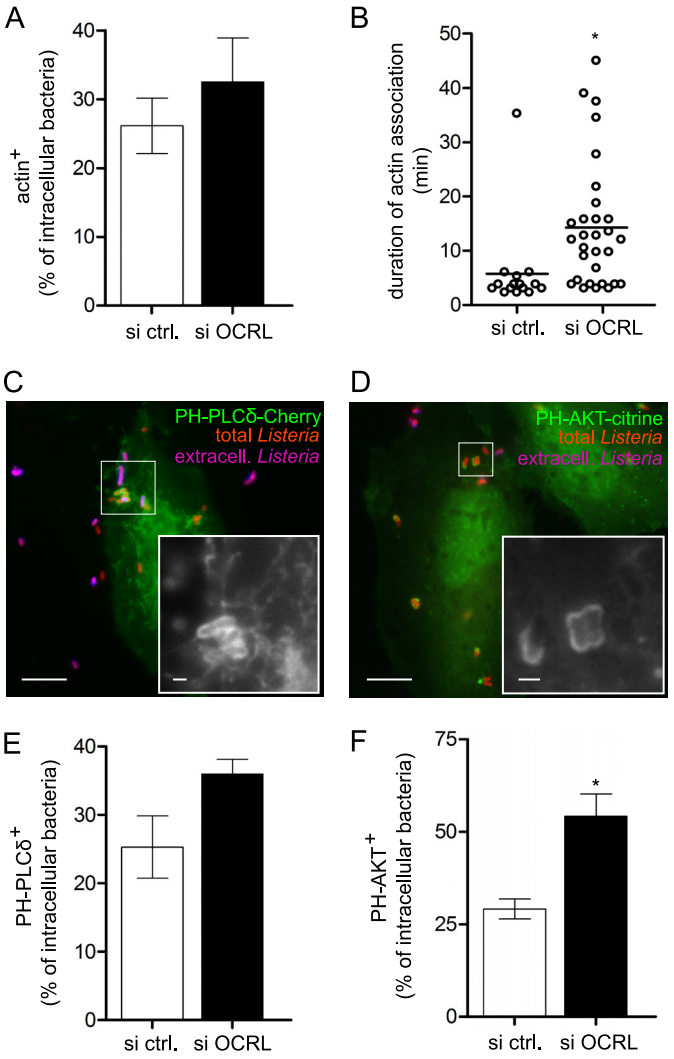

FIGURE 5. **OCRL depletion increases association of actin, PI(4,5)P_2 and PI(3,4,5)P3 to *L. monocytogenes* vacuoles.** *A*, association between actin and intracellular *L. monocytogenes* P14.PrfA* on fixed cells 15 min after infection. Values represent the averages ± S.E. of 4 independent experiments. *si ctrl.*, siRNA control. *B*, time of association of single bacteria to actin visualized by LifeAct-cherry in live-cell imaging experiments; *horizontal bars* indicate the arithmetic mean (Student's *t* test: *, $p < 0.05$). *C*, association between PI(4,5)P_2 visualized by PH-PLC-δ-3-cherry and *L. monocytogenes* P14.PrfA* on fixed cells 25 min after infection. *Bar*: 10 μm (*inset bar*: 1 μm). *D*, association between PI (3,4,5)P_3 visualized by PH-AKT-citrine and *L. monocytogenes* P14.PrfA* on fixed cells 25 min after infection. *Bar*: 10 μm (*inset bar*: 1 μm). *E*, quantification of PH-PLCδ-3-cherry association to intracellular *L. monocytogenes* in fixed cells 25 min after infection. *F*, quantification of PH-AKT-citrine association to intracellular *L. monocytogenes* in fixed cells 25 min after infection Values represent the averages ± S.E. of 3 independent experiments (Student's *t* test: *, $p < 0.05$).

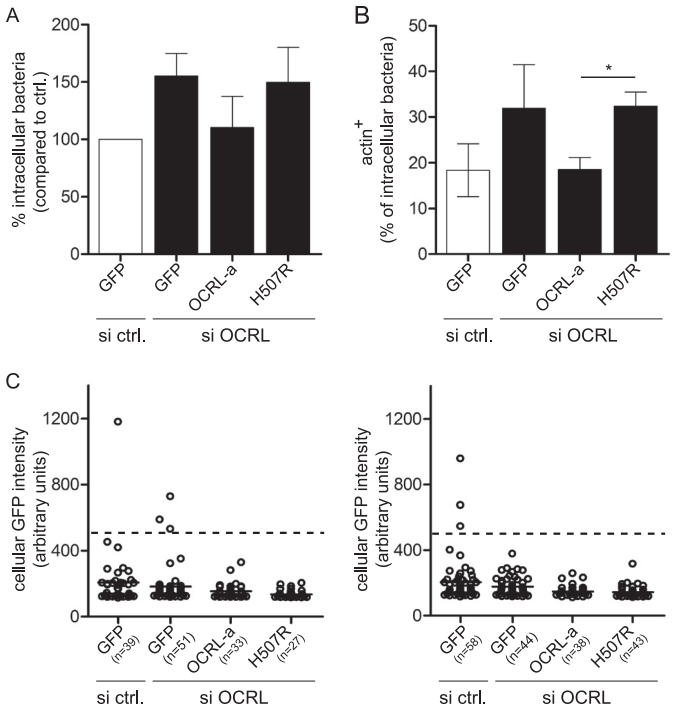

FIGURE 6. **OCRL phosphatase function is responsible for restricting *L. monocytogenes* invasion and for promoting actin depolymerization on bacterial vacuoles.** *A*, one set of HeLa cells was transfected with control siRNA and a plasmid coding for GFP, whereas a second set of HeLa cells was transfected with anti-OCRL siRNA and plasmids coding for GFP, siRNA-resistant pEGFP-OCRL-a, or pEGFP-OCRL-a phosphatase-dead (H507R). After 1 h of infection with *L. monocytogenes* P14.PrfA*, cells were processed for immuno-fluorescence, and invasion was quantified by scoring extracellular *versus* total cell-associated bacteria. Values represent the averages ± S.E. of 3 independent experiments. *si ctrl.*, siRNA control. *B*, transfections were performed as described in *A*, and after 15 min of infection with *L. monocytogenes* P14.PrfA*, cells were processed for immuno-fluorescence microscopy to quantify the percentage of intracellular bacteria associated to actin (labeled by fluorescent phalloidin). Values represent the averages ± S.E. of 3 independent experiments. (Student's *t* test: *, $p < 0.05$.) *C*, the GFP fluorescence intensity of cells chosen for quantifications in *A* and *B* was measured using ImageJ. *Circles* represent cells, and *horizontal lines* represent the average of all cells of the given condition. For quantification, low to medium GFP-expressing cells with a GFP intensity lower than 500 units (*dashed line*) were considered.

compared with cells transfected only with GFP. In a similar assay, we were able to rescue the levels of actin associated to bacterial compartments observed in control cells if EGFP-OCRL-a was overexpressed in OCRL-depleted cells, but no effect was observed when the phosphatase-dead mutant was transfected (Fig. 6*B*). We measured the fluorescence intensity of individual cells expressing low to medium GFP levels in each condition, and we observe that the mean fluorescence level is similar in all the conditions (Fig. 6*C*), suggesting that the transfection levels of the different OCRL variants does not account for the results shown in Fig. 6, *A* and *B*. These results demonstrate therefore that the phosphatase activity of OCRL is responsible for restricting the entry of *L. monocytogenes* by controlling actin dynamics at sites of bacterial internalization.

DISCUSSION

Actin polymerization during invasion of host cells by *L. monocytogenes* is a critical and tightly regulated process. In cells devoid of E-cadherin, entry is mediated by the interaction of InlB with the receptor Met, leading to the recruitment of protein adaptors including Gab1, Cbl, and Shc, which are involved in the translocation of the PI 3-kinase p85-p110 to the plasma membrane (8); production of PI(3,4,5)P_3 leads to the recruitment and activation of Rac1 and Cdc42, which activate proteins such as N-WASP and WAVE, promoting actin polymerization via the Arp2/3 complex (10). Proteins of the enabled/vasodilator stimulated phosphoprotein (Ena/VASP) family, which favor actin filament elongation, are also central to the cellular invasion process (10). Interestingly, actin depolymerization also needs to be tightly regulated, as demonstrated by the observation that perturbation of the actin filament-severing

activity of cofilin (by overexpression of the LIM kinase 1, which phosphorylates and inactivates cofilin) leads to the accumulation of actin cups at sites of bacterial internalization, inhibiting infection (22). The results from the present study demonstrate that the lipid phosphatase OCRL also participates in the *L. monocytogenes* invasion process by restricting invasion through the reduction of the levels of $PI(4,5)P_2$ and $PI(3,4,5)P_3$ at the plasma membrane, therefore moderating local polymerization of actin at bacterial internalization sites. The activity of protein phosphatases such as SHP-1 has been reported to down-regulate phagocytosis (23); however, to our knowledge, OCRL is the first lipid phosphatase reported as being involved in the control of a bacterial internalization process.

At present, only two previous studies have investigated the function of OCRL during bacterial infections (24, 25); however, in both cases, OCRL seems to regulate late intracellular stages of bacterial life within host cells. In one case, it was shown that Dd5P4, which is the *Dictyostelium discoideum* homologue of OCRL, localizes to *Legionella pneumophila*-containing vacuoles and that inactivation of this lipid phosphatase leads to more efficient bacterial replication (24). This result suggests therefore that Dd5P4 restricts *L. pneumophila* replication within *D. discoideum*, and it was hypothesized that the OCRL homologue modifies by a still unidentified pathway the maturation of the bacterial vacuoles, restricting their late interaction with the endoplasmic reticulum (24). In another study, a different scenario was observed during cellular infection by *Chlamydia trachomatis* and *Chlamydia pneumophila*. It was reported that OCRL is recruited to chlamydial inclusions but that inactivation of the lipid phosphatase leads to a decrease in infection, suggesting that OCRL is required for the successful remodeling of the chlamydial inclusions to support bacterial growth (25); production of phosphatidylinositol 4-phosphate by dephosphorylation of $PI(4,5)P_2$ by OCRL at the bacterial inclusion surface seems to be the key step that promotes a positive maturation of the chlamydial inclusion (25).

The role of OCRL in restricting the entry of *L. monocytogenes* in target cells is highly reminiscent of a function recently described for OCRL in the regulation of cytokinesis. Indeed, two recent studies indicate that in human (19) and in *Drosophila* cells (20), the inactivation of OCRL induces a perturbation of $PI(4,5)P_2$ levels leading to cytokinesis failure. Detailed analysis in human cells reveals that higher $PI(4,5)P_2$ levels in OCRL-inactivated cells are associated with abnormal actin levels at the intercellular bridge, which interfere with the completion of cell division (19). In the present work, we report a similar scenario in which we show that the increased levels of $PI(4,5)P_2$ (and also $PI[3,4,5]P_3$) in OCRL-inactivated cells correlate with sustained actin association to bacterial invasion foci, ultimately favoring the entry of *L. monocytogenes* in host cells. $PI(4,5)P_2$ can directly contribute to the activation of several signaling cascades leading to actin polymerization (26). However, as mentioned above, during the internalization of *L. monocytogenes*, production of $PI(3,4,5)P_3$ is a key event that triggers polymerization of actin (7–9). OCRL could modulate bacterial entry both by limiting the plasma membrane levels of $PI(4,5)P_2$ that can be converted to $PI(3,4,5)P_3$ upon InlB-induced Met stimulation and by directly reducing $PI(3,4,5)P_3$ levels, and our results suggest that both mechanisms could act in parallel. However, the sustained association of *L. monocytogenes* with F-actin upon OCRL knockdown does not block entry, as has been observed upon cofilin inactivation, which induces F-actin accumulation beneath invading *L. monocytogenes* and inhibits bacterial internalization (22). We hypothesize that inactivation of cofilin leads to the accumulation of a pool of actin filaments that are nondynamic and therefore cannot support further cytoskeletal rearrangements required for phagosomal dissociation from the plasma membrane, whereas OCRL knockdown does not inhibit actin dynamics, and therefore *L. monocytogenes* phagosome maturation can take place.

Our results concerning the role of OCRL in the restriction of *L. monocytogenes* infection but also in the regulation of the distribution and expression of Met in HeLa cells are in complete agreement with a very recent publication in which it was reported that OCRL depletion impairs the recycling of multiple classes of cell surface receptors that are retained in engorged early endosomes (27). Moreover, trafficking defects are caused precisely by the accumulation of $PI(4,5)P_2$ that promotes an N-WASP-dependent increase in endosomal F-actin (27).

OCRL is a structurally complex protein presenting several domains that promote its association with clathrin, with multiple Rab proteins, as well as with Rac/Cdc42 (16, 28). Our rescue experiment using a phosphatase-dead mutant version of OCRL indicates that the phosphatase activity of the enzyme plays a critical role modulating the association of invading bacteria to the actin cytoskeleton. However, we do not exclude that interaction of OCRL with some of its molecular effectors can also modulate bacterial internalization.

Acknowledgments—We thank Edith Gouin and Roger Zenon for the antibody R217 against the L. monocytogenes 4b strains.

REFERENCES

1. Cossart, P, (2011) Illuminating the landscape of host-pathogen interactions with the bacterium *Listeria monocytogenes. Proc. Natl. Acad. Sci. U.S.A.* **108,** 19484–19491
2. Stavru, F., Archambaud, C., and Cossart, P. (2011) Cell biology and immunology of *Listeria monocytogenes* infections: novel insights. *Immunol. Rev.* **240,** 160–184
3. Mengaud, J., Ohayon, H., Gounon, P., Mege, R.-M., and Cossart, P. (1996) E-cadherin is the receptor for internalin, a surface protein required for entry of *L. monocytogenes* into epithelial cells. *Cell* **84,** 923–932
4. Shen, Y., Naujokas, M., Park, M., and Ireton, K. (2000) InIB-dependent internalization of *Listeria* is mediated by the Met receptor tyrosine kinase. *Cell* **103,** 501–510
5. Pizarro-Cerdá, J., and Cossart, P. (2009) *Listeria monocytogenes* membrane trafficking and lifestyle: the exception or the rule? *Annu. Rev. Cell Dev. Biol.* **25,** 649–670
6. Pizarro-Cerdá, J., and Cossart, P. (2004) Subversion of phosphoinositide metabolism by intracellular bacterial pathogens. *Nat. Cell Biol.* **6,** 1026–1033
7. Ireton, K., Payrastre, B., Chap, H., Ogawa, W., Sakaue, H., Kasuga, M., and Cossart, P. (1996) A role for phosphoinositide 3-kinase in bacterial invasion. *Science* **274,** 780–782
8. Ireton, K., Payrastre, B., and Cossart, P. (1999) The *Listeria monocytogenes* protein InlB is an agonist of mammalian phosphoinositide 3-kinase. *J. Biol. Chem.* **274,** 17025–17032
9. Seveau, S., Tham, T. N., Payrastre, B., Hoppe, A. D., Swanson, J. A., and

Cossart, P. (2007) A FRET analysis to unravel the role of cholesterol in Rac1 and PI 3-kinase activation in the InlB/Met signaling pathway. *Cell. Microbiol.* **9,** 790–803
10. Bierne, H., Miki, H., Innocenti, M., Scita, G., Gertler, F. B., Takenawa, T., and Cossart, P. (2005) WASP-related proteins, Abi1 and Ena/VASP, are required for *Listeria* invasion induced by the Met receptor. *J. Cell Sci.* **118,** 1537–1547
11. Pizarro-Cerdá, J., Payrastre, B., Wang, Y. J., Veiga, E., Yin, H. L., and Cossart, P. (2007) Type II phosphatidylinositol 4-kinases promote *Listeria monocytogenes* entry into target cells. *Cell Microbiol.* **9,** 2381–2390
12. Lowe, M. (2005) Structure and function of the Lowe syndrome protein OCRL1. *Traffic* **6,** 711–719
13. Loi, M. (2006) Lowe syndrome. *Orphanet J. Rare Dis.* **1,** 16
14. Erdmann, K. S., Mao, Y., McCrea, H. J., Zoncu, R., Lee, S., Paradise, S., Modregger, J., Biemesderfer, D., Toomre, D., and De Camilli, P. (2007) A role of the Lowe syndrome protein OCRL in early steps of the endocytic pathway. *Dev. Cell* **13,** 377–390
15. Choudhury, R., Noakes, C. J., McKenzie, E., Kox, C., and Lowe, M. (2009) Differential clathrin binding and subcellular localization of OCRL1 splice isoforms. *J. Biol. Chem.* **284,** 9965–9973
16. Mao, Y., Balkin, D. M., Zoncu, R., Erdmann, K. S., Tomasini, L., Hu, F., Jin, M. M., Hodsdon, M. E., and De Camilli, P. (2009) A PH domain within OCRL bridges clathrin-mediated membrane trafficking to phosphoinositide metabolism. *EMBO J.* **28,** 1831–1842
17. Swan, L. E., Tomasini, L., Pirruccello, M., Lunardi, J., and De Camilli, P. (2010) Two closely related endocytic proteins that share a common OCRL-binding motif with APPL1. *Proc. Natl. Acad. Sci. U.S.A.* **107,** 3511–3516
18. Noakes, C. J., Lee, G., and Lowe, M. (2011) The PH domain proteins IPIP27A and -B link OCRL1 to receptor recycling in the endocytic pathway. *Mol. Biol. Cell* **22,** 606–623
19. Dambournet, D., Machicoane, M., Chesneau, L., Sachse, M., Rocancourt, M., El Marjou, A., Formstecher, E., Salomon, R., Goud, B., and Echard, A. (2011) Rab35 GTPase and OCRL phosphatase remodel lipids and F-actin for successful cytokinesis. *Nat. Cell Biol.* **13,** 981–988
20. Ben El Kadhi, K., Roubinet, C., Solinet, S., Emery, G., and Carréno, S. (2011) The inositol 5-phosphatase dOCRL controls PI(4,5)P_2 homeostasis and is necessary for cytokinesis. *Curr. Biol.* **21,** 1074–1079
21. Pizarro-Cerdá, J., Lecuit, M., and Cossart, P. (2002) Measuring and analyzing invasion of mammalian cells by bacterial pathogens: the *Listeria monocytogenes* system. *Methods Microbiol.* **31,** 161–177
22. Bierne, H. (2001) A role for cofilin and LIM kinase in *Listeria*-induced phagocytosis. *J. Cell Biol.* **155,** 101–112
23. Lawrence, D. W., and Koenig, J. M. (2011) Enhanced phagocytosis in neonatal monocyte-derived macrophages is associated with impaired SHP-1 signaling. *Immunol. Invest.* **41,** 129–143
24. Weber, S. S., Ragaz, C., and Hilbi, H. (2009) The inositol polyphosphate 5-phosphatase OCRL1 restricts intracellular growth of *Legionella*, localizes to the replicative vacuole, and binds to the bacterial effector LpnE. *Cell Microbiol.* **11,** 442–460
25. Moorhead, A. M., Jung, J. Y., Smirnov, A., Kaufer, S., and Scidmore, M. A. (2010) Multiple host proteins that function in phosphatidylinositol-4-phosphate metabolism are recruited to the chlamydial inclusion. *Infect. Immun.* **78,** 1990–2007
26. Yin, H. L., and Janmey, P. A. (2003) Phosphoinositide regulation of the actin cytoskeleton. *Annu. Rev. Physiol.* **65,** 761–789
27. Vicinanza, M., Di Campli, A., Polishchuk, E., Santoro, M., Di Tullio, G., Godi, A., Levtchenko, E., De Leo, M. G., Polishchuk, R., Sandoval, L., Marzolo, M., and De Matteis, M. A. (2011) OCRL controls trafficking through early endosomes via PtdIns4,5P_2-dependent regulation of endosomal actin. *EMBO J.* **30,** 4970–4985
28. Hou, X., Hagemann, N., Schoebel, S., Blankenfeldt, W., Goody, R. S., Erdmann, K. S., and Itzen, A. (2011) A structural basis for Lowe syndrome caused by mutations in the Rab-binding domain of OCRL1. *EMBO J.* **30,** 1659–1670